A Ray-Tracing Algorithm Based on the Computation of (Exact) Ray Paths With Bidirectional Ray-Tracing

Mehmet Mert Taygur, *Member, IEEE*, and Thomas F. Eibert, *Senior Member, IEEE*

***Abstract*— A novel ray-tracing algorithm to cope with the phase errors due to incorrect ray path computations in ray-launching approaches is presented. The algorithm utilizes bidirectional ray-tracing to collect information about wavefronts incident on an interaction surface and yields considerable improvements in accuracy compared to conventional unidirectional ray-tracing. The points, where exact ray paths intersect with the surface, are obtained according to the Fermat principle of least time. If the interaction surface is aligned with diffraction edges, the corresponding critical points of the second kind can also be retrieved and complicated diffraction treatments by shooting diffracted rays on Keller cones can be avoided. Thus, a substantial reduction in the number of rays can be achieved. Furthermore, a typical problem encountered in traditional ray-tracing due to the reception sphere mechanism, i.e., incorrect ray contributions, can mostly be evaded. Numerical results demonstrate the capabilities of the new algorithm and its advantages against traditional techniques.**

***Index Terms*— Asymptotic expansion, diffraction, Fermat principle, ray-tracing, reciprocity, stationary point.**

I. Introduction

THE ever-increasing demand for superior performance in wireless networks has generated considerable interest in the utilization of millimeter-wave systems since much larger bandwidths can be leveraged to achieve higher data rates. In the last decades, ray-tracing simulations have emerged as a useful method to design/analyze such systems, not only in wireless applications but also in many radar applications [1], [2]. The simulations are most commonly based on the shooting and bouncing rays (SBR) algorithm [3] where a large number of rays are sent from the transmitter, and a sphere placed at the receiver location is utilized for the reception test. Even though ray-tracing simulations based on the SBR algorithm have notable advantages compared to many other simulation techniques, the approach is not without drawbacks. In particular, the number of ray launches usually has to be significantly increased in order to maintain a certain level of accuracy as the scenario becomes larger or more complex since the reception spheres usually have to be kept small in size in order to prevent incorrect ray contributions [4]. Several studies have dealt with this problem by introducing adaptive ray-launching algorithms. A commonly utilized method is to perform multiple consecutive simulations with a relatively small number of ray launches where the launch directions at each step are determined according to the directions of the rays which hit the receiver at the previous steps. Thus, the feasible ray paths between a receiver and a transmitter can be obtained in an iterative manner [5]–[8]. Various studies have approached the problem from a slightly different perspective, where ray-tracing is considered as minimization of the optical path length, in accordance with the Fermat principle of least time [9], [10]. Although these techniques can effectively be utilized to alleviate the complexity issues, an improper choice of the sphere size and the number of ray launches may have further implications at millimeter-wave frequencies which were not sufficiently addressed in these studies. More specifically, large reception spheres may yield minor inaccuracies in the path lengths of the received rays. Since the wavelength is also very small, even these minor errors in the path length can result in significant phase errors. The problem has been acknowledged in [11] for a terahertz propagation scenario where the computation of the ray paths was based on minimizing the optical path length.

The phase error problem can easily manifest itself as well at lower frequencies (e.g., in the millimeter-wave regime), but the significance of the problem in such situations is neither covered satisfactorily in the literature, nor were more realistic propagation environments considered, such as diffraction scenarios or urban-like landscapes with strong shadowing effects.

In order to address these issues, a new algorithm based on bidirectional ray-tracing is presented where the properties of the exact ray paths and the transfer functions are computed by using a small number of rays collected on an interaction surface [4], [12]. The primary strength of the proposed method is that the path length can be computed much more accurately compared to the conventional techniques based on reception spheres; hence, phase errors due to the imperfect path length information are significantly diminished. Another important advantage of the new approach is its effectiveness in reducing the complexity of the simulation process by avoiding Keller cones for edges that are aligned with the interaction surface. In addition to the benefits regarding reduced computation times and smaller phase errors, the problems related

Manuscript received November 4, 2019; revised January 23, 2020; accepted March 22, 2020. Date of publication April 2, 2020; date of current version August 4, 2020. *(Corresponding author: Mehmet Mert Taygur.)*

The authors are with the Chair of High-Frequency Engineering, Technical University of Munich, 80290 Munich, Germany (e-mail: hft@ei.tum.de).

Color versions of one or more of the figures in this article are available online at http://ieeexplore.ieee.org.

Digital Object Identifier 10.1109/TAP.2020.2983775

0018-926X © 2020 IEEE. Personal use is permitted, but republication/redistribution requires IEEE permission.
See https://www.ieee.org/publications/rights/index.html for more information.

Authorized licensed use limited to: University at Buffalo Libraries. Downloaded on October 08,2023 at 04:39:01 UTC from IEEE Xplore. Restrictions apply.

to the acquisition of incorrect ray contributions can mostly be avoided as well. Thus, some of the most critical issues, which are associated with the traditional ray-tracing, can be circumvented in a single method.

II. Conventional Reception Methods and Considerations for High Frequencies

Ray-tracing methods are based on field representations under high-frequency assumptions, i.e., the wavenumber tends to infinity. The rays indicate the propagation directions of electromagnetic waves where astigmatic wavefronts are considered in general. The electric and magnetic fields and the propagation of the waves can be represented by [4]

$$\mathbf{E} = \hat{\mathbf{e}} E_0 \sqrt{\frac{\rho_1 \rho_2}{(\rho_1 + d)(\rho_2 + d)}} e^{-jkd}, \quad \mathbf{H} = \sqrt{\frac{\epsilon}{\mu}}\, \hat{\mathbf{k}} \times \mathbf{E} \quad (1)$$

where $d \in \mathbb{R}$ denotes the distance for which the wave propagates from a reference point, ρ_1 and ρ_2 are the radii of curvature of the astigmatic wave at the reference point, k is the wavenumber, ϵ and μ are the dielectric permittivity and the magnetic permeability of the propagation medium, respectively, $\hat{\mathbf{e}}$ and $\hat{\mathbf{k}} \in \mathbb{R}^3$ are orthonormal vectors which represent the polarization of the electric field and the propagation direction, respectively. Note that the field expressions are assumed to be time-harmonic with a suppressed time dependence of $e^{j\omega t}$, where ω is the angular frequency.

In complex scenarios, such as urban environments, the computation of the ray paths typically relies on the SBR algorithm [13], [14]. A large number of ray launches are commonly utilized as the rays are traced throughout the geometry after the launch and checked whether they reach a receiver. The reception test involves an inquiry about whether the rays intersect with a sphere (commonly known as the reception sphere) placed at the receiver location [15]. The size of the reception sphere is an important parameter here, and it should be chosen carefully in order to ensure that the simulation results are sufficiently accurate [12], [16]. Even though many studies have comprehensively addressed this problem previously, the scenarios, where high frequencies (e.g., millimeter-waves) are utilized, constitute additional difficulties which were not thoroughly considered before. A major challenge in such cases is to determine the ray path lengths correctly, as even the slightest errors in the path length calculation might yield a large phase change due to the short wavelength (see Fig. 1).

It should be noted that similar problems may occur in scenarios that involve diffractions since the diffraction paths are identified in a similar way as the received rays are found, i.e., utilizing cylinders lying along the diffraction edges. Selecting a smaller radius (i.e., on the order of the wavelength) and launching an accordingly large number of rays can solve these problems. However, this comes at the expense of the computational load, which depends on the number of ray launches. Therefore, more sophisticated solutions, which can provide accurate ray path information without significant computational burden, are needed.

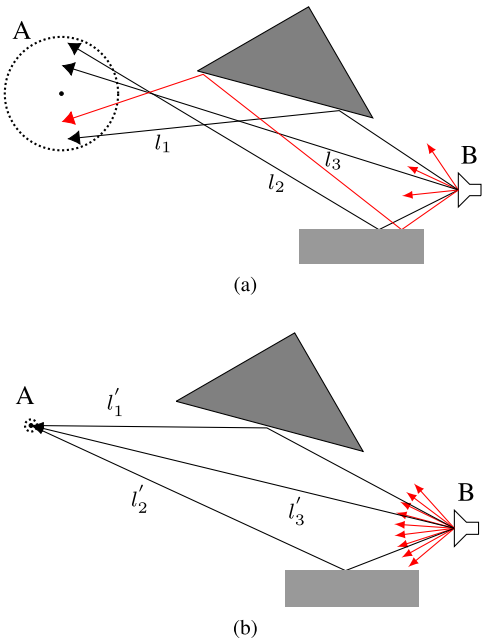

Fig. 1. Comparison of two unidirectional ray-tracing simulations with (a) large and (b) small reception spheres as well as different numbers of ray launches. The scenario in (a) comprises a large sphere with a small number of ray launches, causing errors in the computation of the ray path lengths, in addition to an incorrect ray contribution.

III. Identifying Stationary Points

Computation of the exact ray paths in a ray-tracing simulation essentially means the utilization of the Fermat principle of least time, which can be written as [17], [18]

$$s = \int n(\mathbf{r}) dl \quad (2)$$

where $\mathbf{r} \in \mathbb{R}^3$ is the coordinate vector, s and $n(\mathbf{r})$ denote the ray path length and the refractive index of the propagation medium, respectively. Assuming a scenario with homogeneous medium (e.g., free space), the trajectory of a ray, which passes through this medium, can be represented as a straight line. Since the length of a ray path is stationary with respect to variations of the path, identifying the exact ray path can be considered as an optimization problem.

Let us consider a simple free-space propagation scenario, where A and B are two antennas, and Ψ is a surface between A and B. If certain properties of the waves, which would be generated by A and B, are known on the surface, then it is possible to identify a point on Ψ such that the ray, which links A and B (only a single ray exists in this specific scenario since there are no scatterers in the environment), passes through the point. In other words, the location, where the exact ray path intersects with the surface, can be determined by using the knowledge about the incident waves on the surface. The information, which is needed to find this stationary point, are the radii of curvature of the incident wavefronts. On the other hand, the field-related information associated with each wavefront is used for evaluating the transfer function once the stationary point has been identified. The required data to obtain

Authorized licensed use limited to: University at Buffalo Libraries. Downloaded on October 08,2023 at 04:39:01 UTC from IEEE Xplore. Restrictions apply.

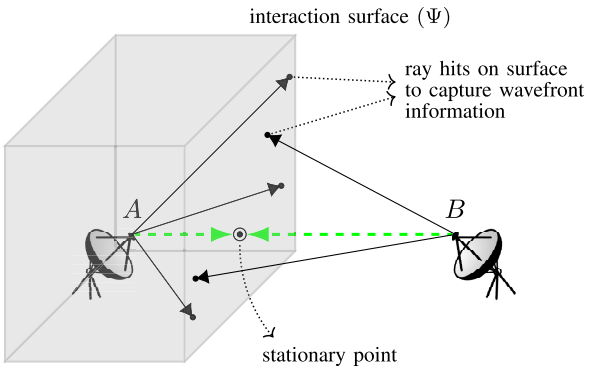

Fig. 2. Identification of the stationary point on the interaction surface by using the bidirectional ray-tracing technique.

the stationary point and the field expressions are acquired by launching rays from both receiver and transmitter sites and collecting these rays on the surface Ψ, i.e., by a bidirectional ray-tracing approach.

A. Bidirectional Ray-Tracing

Bidirectional ray-tracing involves ray-launching from both receiver and transmitter sites, in contrast to conventional ray-tracing (which can be called unidirectional ray-tracing) [19]. The bidirectional ray-tracing technique differs from unidirectional ray-tracing in terms of the reception mechanism, since both antennas are utilized for ray-launching, and the rays are captured on an interaction surface rather than a small reception sphere. Ideally, the interaction surface completely encloses one of the antennas; however, many special cases are possible based on the particular consideration [4], [12], [19].

The main aim of the bidirectional ray-tracing process is to collect information about the incident waves on the interaction surface (Fig. 2). As the rays, which are associated with a particular wavefront, hit the interaction surface, certain information such as the propagation direction or radii of curvature of the astigmatic wavefront, can be obtained at the intersection point. By using this information, it is possible to calculate the optical path length for any point on the interaction surface (as for a ray, which hits, after it was really launched and traced). As the path length for both antennas can be obtained at any point on the surface, the quantity to minimize is simply the sum of these two path length values. Note that only a single unique wavefront from both sites is considered here. In the case of multiple wavefronts though, each distinct wavefront pair should be examined independently for the presence of stationary points, i.e., a separate stationary point inquiry (as well as transfer function calculation, if the point exists) should be performed for each wavefront pair.

B. Minimization of the Path Length

The stationary points satisfy the Fermat principle of least time, where the sum of the ray path lengths for receiver and transmitter rays is minimum, as stated before. The directions of the receiver and transmitter rays are usually opposite (i.e., the inner product of the normalized propagation vectors equals -1) at the minima, although exceptions may occur in nonline-of-sight propagation paths as the minima may be located at the junction between the interaction surface and an object in the environment. For such cases, the problem can be considered as finding the minimum according to the geometrical constraints where the ray path constitutes a critical point of the second kind. The pseudocode for the minimization algorithm is shown in Algorithm 1. The minimization

Algorithm 1 Ray Path Length Computation and Minimization

procedure MINIMIZELENGTH
  $\mathbf{d}_1, \mathbf{d}_2 \leftarrow$ orthonormal vectors on the surface
  $\mathbf{c} \leftarrow$ surface center point
  repeat
    $l_0 \leftarrow$ pathLength($\mathbf{c}$)
    $\alpha \leftarrow$ pathLength($\mathbf{c} + \epsilon\mathbf{d}_1$) $- l_0$ ▷ $0 < \epsilon \ll \lambda$
    repeat
      $\alpha \leftarrow k\alpha$ ▷ faster convergence often for $k > 1$
      $l_1 \leftarrow$ pathLength($\mathbf{c} - \alpha\mathbf{d}_1$)
    until $l_1 > l_0$ or max. iteration limit
    $\mathbf{c} \leftarrow \mathbf{c} - \mathbf{d}_1\alpha/k$
    $l_1 \leftarrow$ pathLength($\mathbf{c}$)
    $\alpha \leftarrow$ pathLength($\mathbf{c} + \epsilon\mathbf{d}_2$) $- l_1$
    repeat
      $\alpha \leftarrow k\alpha$
      $l_2 \leftarrow$ pathLength($\mathbf{c} - \alpha\mathbf{d}_2$)
    until $l_2 > l_1$ or max. iteration limit
    $\mathbf{c} \leftarrow \mathbf{c} - \mathbf{d}_2\alpha/k$
    $l_2 \leftarrow$ pathLength($\mathbf{c}$)
  until $l_2 \geq l_0$
  if $\mathbf{c}$ outside the surface **then**
    $\mathbf{c} \leftarrow \arg\min_{\partial\Psi} \|\partial\Psi - \mathbf{c}\|$ ▷ $\partial\Psi$: boundary of Ψ
  end if
  $l_2 \leftarrow$ pathLength($\mathbf{c}$)
  return $\mathbf{c}, l_2$
end procedure
procedure PATHLENGTH($\mathbf{c}$)
  for both wavefronts from A and B **do**
    ▷ path length is sought at $\mathbf{c}$
    ▷ let r be a ray, which is associated with a particular wavefront and whose properties are known.
    $\rho_{1,\mathrm{r}},\ \rho_{2,\mathrm{r}}$ ▷ radii of curvature
    $\mathbf{P}_r,\ \mathbf{d}_r$ ▷ hit point and incident direction
    $\mathbf{S} \leftarrow \mathbf{P}_r - \rho_{2,\mathrm{r}}\mathbf{d}_r - \left(\rho_{1,\mathrm{r}} - \rho_{2,\mathrm{r}}\right)\mathbf{T}_r\mathbf{d}_r$
    ▷ $\mathbf{T}_r$ represents rotation of the propagation direction vector at a diffraction edge (identity matrix, if no diffraction).
    if $\rho_{1,\mathrm{r}} = \rho_{2,\mathrm{r}}$ **then** ▷ no diffraction
      $l_{\{A,B\}} \leftarrow \|\mathbf{S} - \mathbf{c}\|$
    else
      $\mathbf{M} \leftarrow$ arbitrary point on edge
      $l_{\{A,B\}} \leftarrow \min_{\mathbf{M}} \|\mathbf{S} - \mathbf{M}\| + \|\mathbf{c} - \mathbf{M}\|$
    end if
  end for
  return $l_A + l_B$
end procedure

Authorized licensed use limited to: University at Buffalo Libraries. Downloaded on October 08,2023 at 04:39:01 UTC from IEEE Xplore. Restrictions apply.

algorithm is based on a line search method where a step size value for the direction vectors is computed iteratively. In order to ensure that the computed minimum point lies inside the boundaries of the given surface, a correction step is performed when necessary. The path length calculation algorithm utilizes the information on the propagation direction and the radii of curvature of the incident astigmatic wavefronts from both sites. If diffractions are involved in the simulation, then additional information, such as edge orientation or angular difference between incoming and outgoing rays, are also utilized.

IV. Computation of Antenna Transfer Function

The computation of the antenna transfer function is based on the application of the reciprocity theorem [4]. Referring to the configuration in Fig. 2, let A and B be two antennas, designated as receiver and transmitter, respectively, and Ψ be a surface closed around A. By using the reciprocity theorem and applying the common port voltage/current representation, the induced open-circuit voltage at the ports of antenna A (V_A^{oc}) is given as [20], [21]

$$\frac{-1}{I_A}\oiint_{\Psi}[(\mathbf{H}_A\times\mathbf{E}_B)-(\mathbf{H}_B\times\mathbf{E}_A)]\cdot d\mathbf{S}=V_A^{oc} \tag{3}$$

where I_A is the port current at antenna A on transmit, $\mathbf{E}_A$, $\mathbf{H}_A$ and $\mathbf{E}_B$, $\mathbf{H}_B$ are electric and magnetic transmitted fields from A and B, respectively. The antenna transfer function is obtained by evaluating the reciprocity integral in (3), assuming that the generator voltage at antenna B is already known. Although the reciprocity theorem states that the surface, on which the electric and magnetic fields are evaluated, should be closed, it is known that a large open surface can also be utilized to compute the transfer function in certain cases, as demonstrated in [4].

It is presumed that the field expressions are known at specific points on the surface in order to evaluate the reciprocity integral in (3). Since a single ray can provide the field information for only the point where it interacts with the surface, a convenient way to obtain the field expressions at any arbitrary point on the surface (the points which are essential for evaluating the integral) is interpolation. The interpolation method utilized in this study can be found in [4].

The reciprocity integral in (3) consists of oscillatory phase terms which are dependent on the propagation constant. The integral can be represented in a more general form by [22]

$$\iint_{\Psi}[(\mathbf{H}_A\times\mathbf{E}_B)-(\mathbf{H}_B\times\mathbf{E}_A)]\cdot d\mathbf{S}=\iint_{\Psi}f(\mathbf{r})e^{jkg(\mathbf{r})}dS \tag{4}$$

with

$$\begin{aligned}\Theta(\mathbf{r})&=\left[(\mathbf{H}_A(\mathbf{r})\times\mathbf{E}_B(\mathbf{r}))-(\mathbf{H}_B(\mathbf{r})\times\mathbf{E}_A(\mathbf{r}))\right]\cdot\hat{\mathbf{n}}\\ g(\mathbf{r})&=\arg(\Theta(\mathbf{r}))/k,\quad f(\mathbf{r})=|\Theta(\mathbf{r})|\end{aligned} \tag{5}$$

where $\hat{\mathbf{n}}$ is the unit surface normal vector for Ψ, $g(\mathbf{r})$ is the phase function (which is smooth and does not contain discontinuities), $f(\mathbf{r})$ is the magnitude function, and k is the propagation constant. Such an integral might be tedious to evaluate with an algorithm whose complexity may scale with the wavelength. Asymptotic techniques can be applied for solving the problem efficiently, and the result can be represented in terms of the values of f and g as well as their derivatives at the particular point where $\nabla g=0$ [23], [24]. The function g represents the variation of the phase of the field expressions for both antennas but the variation of the optical path lengths typically has a much greater influence on g than other factors, such as antenna patterns. Therefore, the point where $\nabla g=0$ is considered as the minimum of the optical path length. The phase function g can thus be expressed as

$$g=g_{\text{tx,path}}(\mathbf{r})+g_{\text{rx,path}}(\mathbf{r})+\frac{g_c(\mathbf{r})}{k} \tag{6}$$

where $g_{\text{tx,path}}$ and $g_{\text{rx,path}}$ denote the optical path lengths for the transmitter and the receiver waves, respectively, and g_c can be described as an additional phase shift term which is independent of the path length (depends typically on antenna patterns and diffraction coefficients, if any). Here, it is noticed that the problem is consistent with the definition of the stationary point described in Section III (in the context of asymptotic analysis, the term *stationary phase point* can also be utilized). Hence, the asymptotic expansion of (4) as $k\to\infty$ can be given by [25], [26]

$$I\sim\frac{2\pi f(\mathbf{r}_0)}{k\sqrt{\det(\text{Hess}(g(\mathbf{r}_0)))}}e^{jkg(\mathbf{r}_0)+j\pi/4}+\mathcal{O}(k^{-1}) \tag{7}$$

where det(.) and Hess(.) are determinant and Hessian operators, respectively. The propagation direction of the rays from the receiver and transmitter sites are typically opposite to each other at the stationary phase point; in other words, $\mathbf{d}_A(\mathbf{r}_0)\cdot\mathbf{d}_B(\mathbf{r}_0)=-1$, where $\mathbf{d}_A$ and $\mathbf{d}_B$ denote the propagation direction for the receiver and transmitter antennas, respectively.

The computation of the asymptotic expressions in (7) requires the knowledge of the derivatives of the phase function g. A prevalent approach for computing the derivative numerically is to utilize the finite difference method. However, it is well-known that numerical implementations of the finite difference approach might be problematic if the step-size is not selected correctly, i.e., rounding errors or discretization errors may occur [27], [28]. In order to avoid such issues, an alternative solution method, which relies on the fact that the transfer function is independent of the surface orientation (assuming that the environment and the relative positions of the antennas do not change), is utilized. In order to illustrate the situation better, let us consider two different interaction surface configurations, as depicted in Fig. 3, where the main problem is to obtain the transfer function by using the asymptotic expansion (7) for the second scenario. Note that the first scenario is assumed to comprise exactly the same environment as the second, with the only exception that the exact ray path is perpendicular to the interaction surface, i.e., the surface normal is parallel to the propagation direction vectors ($|\mathbf{d}_A\cdot\hat{\mathbf{n}}_1|=1$ $|\mathbf{d}_B\cdot\hat{\mathbf{n}}_1|=1$). The location of the stationary phase point is also assumed to be the same and denoted by $\mathbf{r}_0$; thus, the field expressions and the properties of the wavefronts, such as the radii of curvature, are identical at $\mathbf{r}_0$. Given that the propagation environment and the locations of the receiving and transmitting antennas remain constant, the received voltage should be identical for both cases whereas

Authorized licensed use limited to: University at Buffalo Libraries. Downloaded on October 08,2023 at 04:39:01 UTC from IEEE Xplore. Restrictions apply.

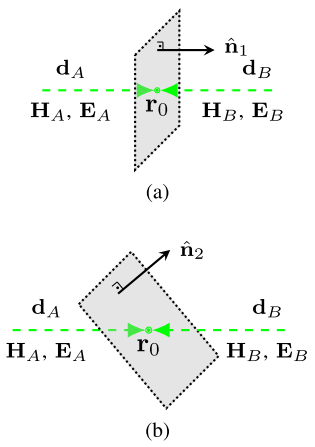

Fig. 3. Illustration of two distinct surface configurations having different orientations with respect to the incident ray directions.

the individual terms of (7), such as the magnitude function (f) or the Hessian operation on the phase function (Hess(g)) can be different. Let us now denote the Hessian terms by $\mathbf{q}_1$ and $\mathbf{q}_2$, and the magnitude functions by f_1 and f_2, for the first and second configurations, respectively. The relation between these quantities can then be given by

$$\begin{aligned} |I| &= \frac{2\pi f_1(\mathbf{r}_0)}{k\sqrt{\det(\mathbf{q}_1(\mathbf{r}_0))}} = \frac{2\pi f_2(\mathbf{r}_0)}{k\sqrt{\det(\mathbf{q}_2(\mathbf{r}_0))}} \\ &\rightarrow \frac{f_1(\mathbf{r}_0)}{\sqrt{\det(\mathbf{q}_1(\mathbf{r}_0))}} = \frac{f_2(\mathbf{r}_0)}{\sqrt{\det(\mathbf{q}_2(\mathbf{r}_0))}} \\ &\rightarrow \sqrt{\det(\mathbf{q}_2(\mathbf{r}_0))} = \sqrt{\det(\mathbf{q}_1(\mathbf{r}_0))}\,\frac{f_2(\mathbf{r}_0)}{f_1(\mathbf{r}_0)}. \end{aligned} \tag{8}$$

It is now shown that f_1 and $\mathbf{q}_1$ may be written without any dependence on the surface orientation. The Hessian term for the first configuration can in general be written in terms of the radii of curvature of the incident wavefronts by

$$\mathbf{q}_1(\mathbf{r}_0) = \begin{bmatrix} \dfrac{1}{\rho_{1,A}(\mathbf{r}_0)} + \dfrac{1}{\rho_{1,B}(\mathbf{r}_0)} & 0 \\ 0 & \dfrac{1}{\rho_{2,A}(\mathbf{r}_0)} + \dfrac{1}{\rho_{2,B}(\mathbf{r}_0)} \end{bmatrix} \tag{9}$$

where ρ_1 and ρ_2 denote the radii of curvature for the astigmatic wavefronts, and the subscripts A and B denote where the wavefronts originate from (either antenna A or B). Finally, the magnitude function f_1 can be given to complete (8)

$$f_1 = |[(\mathbf{H}_A(\mathbf{r}_0) \times \mathbf{E}_B(\mathbf{r}_0)) - (\mathbf{H}_B(\mathbf{r}_0) \times \mathbf{E}_A(\mathbf{r}_0))] \cdot \hat{\mathbf{n}}_1| \tag{10}$$

where $\hat{\mathbf{n}}_1$ is the surface normal for the first scenario. Note that the surface normal can be replaced by $\mathbf{d}_A$ or $\mathbf{d}_B$, since the surface normal vector is parallel to the propagation direction vectors in this particular scenario. The asymptotic expansion valid for both scenarios can be written as

$$I \sim \frac{2\pi f_1\ e^{jkg(\mathbf{r}_0)+j\pi/4}}{k\sqrt{\left(\frac{1}{\rho_{1,A}(\mathbf{r}_0)} + \frac{1}{\rho_{1,B}(\mathbf{r}_0)}\right)\left(\frac{1}{\rho_{2,A}(\mathbf{r}_0)} + \frac{1}{\rho_{2,B}(\mathbf{r}_0)}\right)}} \tag{11}$$

with

$$g(\mathbf{r}_0) = \arg([(\mathbf{H}_A(\mathbf{r}_0) \times \mathbf{E}_B(\mathbf{r}_0)) - (\mathbf{H}_B(\mathbf{r}_0) \times \mathbf{E}_A(\mathbf{r}_0))] \cdot \hat{\mathbf{n}}_2)/k. \tag{12}$$

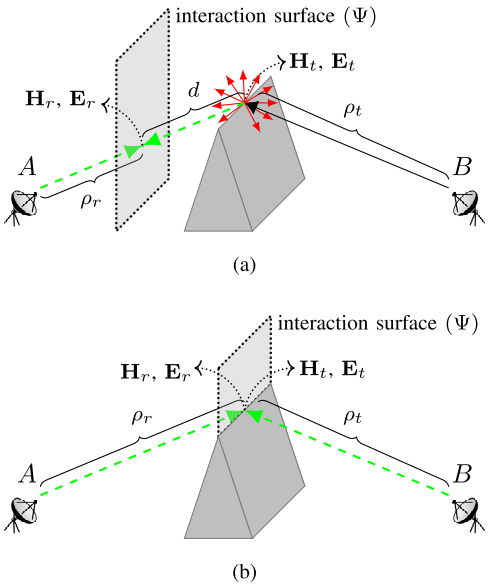

Fig. 4. Surface configuration for diffraction scenarios and positioning the surface over the edge to eliminate the need for Keller cones.

In conclusion, the asymptotic expansion can be written in terms of the quantities which can be extracted from the geometry and wavefront characteristics, without performing any numerical derivative calculation.

A. Considerations for Diffraction Scenarios

A commonly encountered situation in realistic propagation scenarios is the presence of dominant paths which involve wedge diffraction. The placement of the interaction surface plays a crucial role here since the simulation of such scenarios typically involves Keller cones, which might cause an enormous growth in the ray-tree, thereby increasing the computational load [4], [29]. We first consider an environment where the receiver and transmitter antennas are separated by a wedge, and a large, open interaction surface is placed near the wedge at the receiver site, such that the diffracted rays immediately reach the surface (i.e., no further interactions, such as reflections, happen after the diffraction). Evidently, the scenario involves uniform theory of diffraction (UTD)-based computations and a stationary phase point exists on the surface. Let us also assume that the incident fields upon the edge from the transmitter site A are given by $\mathbf{H}_r$, $\mathbf{E}_r$, and the fields at the stationary phase point from the receiver site B are given by $\mathbf{H}_t$, $\mathbf{E}_t$. Then, the asymptotic expansion can be written as

$$\begin{aligned} \Theta &= \left[\mathbf{H}_r \times \left(\mathbf{E}_t \cdot \bar{\mathbf{D}}\sqrt{\frac{\rho_t}{d(d+\rho_t)}}\right) \right. \\ &\quad \left. - \left(\mathbf{H}_t \cdot \bar{\mathbf{D}}\sqrt{\frac{\rho_t}{d(d+\rho_t)}}\right) \times \mathbf{E}_r\right] \cdot \mathbf{d}, \quad g = \arg(\Theta) \\ I &\sim \frac{2\pi\ |\Theta| e^{jkg+j\pi/4}}{k\sqrt{\left(\frac{1}{\rho_r} + \frac{1}{\rho_t+d}\right)\left(\frac{1}{\rho_r} + \frac{1}{d}\right)}} \end{aligned} \tag{13}$$

Although the transfer function can be accurately calculated in that way, it may not be the computationally most efficient

Authorized licensed use limited to: University at Buffalo Libraries. Downloaded on October 08,2023 at 04:39:01 UTC from IEEE Xplore. Restrictions apply.

approach due to the growth of the ray-tree with Keller cones. Our approach is, therefore, to eliminate the need for Keller cones by reducing the distance between the diffraction point and the interaction surface to zero, such that the interaction surface coincides with the edge (see Fig. 4). Thus, the transfer function can be calculated by using the incident rays from transmitter and receiver sites and applying the UTD coefficients accordingly. This can be achieved by removing the indeterminate expressions at the numerator (divergence factors for the diffracted fields) and the denominator (Hessian term) of (13) by an algebraic elimination. Thus, a well-defined result is obtained in the form of

$$\lim_{d\to 0} I \sim \frac{2\pi \left| \left[\mathbf{H}_r \times \left(\mathbf{E}_t \cdot \bar{\mathbf{D}}\right) - \left(\mathbf{H}_t \cdot \bar{\mathbf{D}}\right) \times \mathbf{E}_r\right] \cdot \mathbf{d} \right|}{k\sqrt{\left(\frac{1}{\rho_r} + \frac{1}{\rho_t}\right)}} e^{jkg + j\pi/4}. \tag{14}$$

Note that the Keller cones can be eliminated in this way, which is a major advantage of our approach in terms of computational complexity

B. Special Cases

Shadowing effects can be observed very often in propagation environments with many scatterers (e.g., dense urban scenarios), as the typical outcome is the partial illumination of the interaction surface, i.e., the rays, which are associated with a particular wavefront, may not reach every point on the interaction surface. Consequently, a stationary point might be found, as if a ray path could pass through that point, where, in fact, such a path cannot exist, i.e., it is blocked by the surrounding objects. In such a case, two different approaches can be adopted to solve the problem. In the first approach, an iterative ray-launching solution can be applied where new rays are sent toward the identified stationary points. The second approach involves the validation of the stationary point and a nonasymptotic integration process in certain cases. In this study, the latter approach is utilized.

C. Complexity Considerations

Due to the complexity of ray-tracing approaches, numerical complexity considerations are generally difficult and not very accurate. The methods presented in this article result in considerable speed-ups as compared to the approach in [4].

V. Numerical Results

A. Two-Ray Reflection and Knife-Edge Diffraction Scenarios

Two test scenarios were simulated for 10 different frequencies between 2.5 and 25 GHz (with linearly varying steps), and the accuracy of the proposed method is compared to the classic unidirectional ray-tracing algorithm. The illustrations of ground reflection and knife-edge diffraction scenarios are given in Figs. 5 and 6, respectively (note that the figures include the interaction surfaces, which are of course not part of the unidirectional ray-tracing simulations). Both scenarios involve a transmitter at a fixed location and a receiver

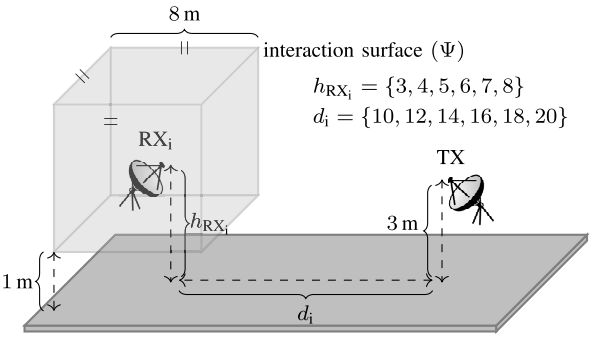

Fig. 5. Two-ray ground reflection scenario illustration.

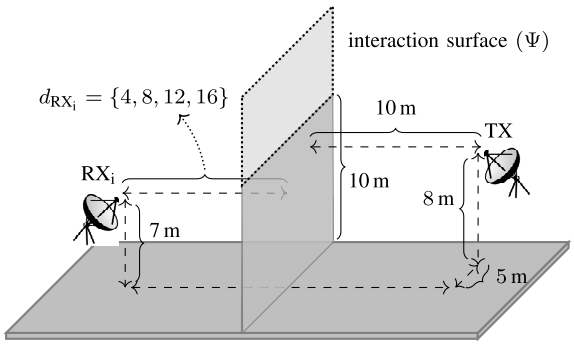

Fig. 6. Knife-edge diffraction scenario illustration.

whose location changes. In the former case, six different receiver locations were considered, whereas the latter case involves four different receiver locations. It can be seen that the diffraction scenario includes a ground plane; thus, four unique ray paths occur (diffraction, reflection-diffraction, diffraction-reflection, reflection-diffraction-reflection), compared to the two paths in the ground reflection environment. Both environments are assumed to have perfect electric conductor material throughout the geometry. The parameters, namely, the number of the ray launches and the reception sphere size, were chosen as follows: first, the values which yield an error below 1 dB at 2.5 GHz for all receivers in the unidirectional ray-tracing simulation, are determined. The number of the rays is kept as small as possible under this accuracy constraint (in the knife-edge diffraction scenario, the size of the diffraction cylinder and the number of the emerging rays over Keller cones were also taken into account). Afterward, the same settings were used for all the frequency points up to 25 GHz. To establish a fair comparison, the same number of ray launches was utilized in the proposed method as well (i.e., the sum of the number of ray launches from the receiver and transmitter sites). The performance measure was assumed to be the deviation of the antenna transfer function (i.e., the ratio of the induced voltage at the receiving antenna port and the generator voltage of the transmitting antenna) from the reference simulation, which is based on a unidirectional ray-tracing simulation with small reception spheres and small diffraction cylinders as well as a large number of ray launches. The results for the ground reflection and diffraction scenarios are shown in Figs. 8 and 9, respectively.

Authorized licensed use limited to: University at Buffalo Libraries. Downloaded on October 08,2023 at 04:39:01 UTC from IEEE Xplore. Restrictions apply.

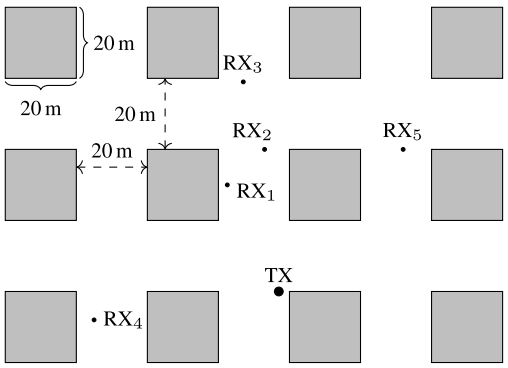

Coordinates: TX:(0,0), RX_1:(-14.5,30), RX_2:(-4,40), RX_3:(-10,59), RX_4:(-52,-8), RX_5:(35,40)

Fig. 7. Urban scenario illustration.

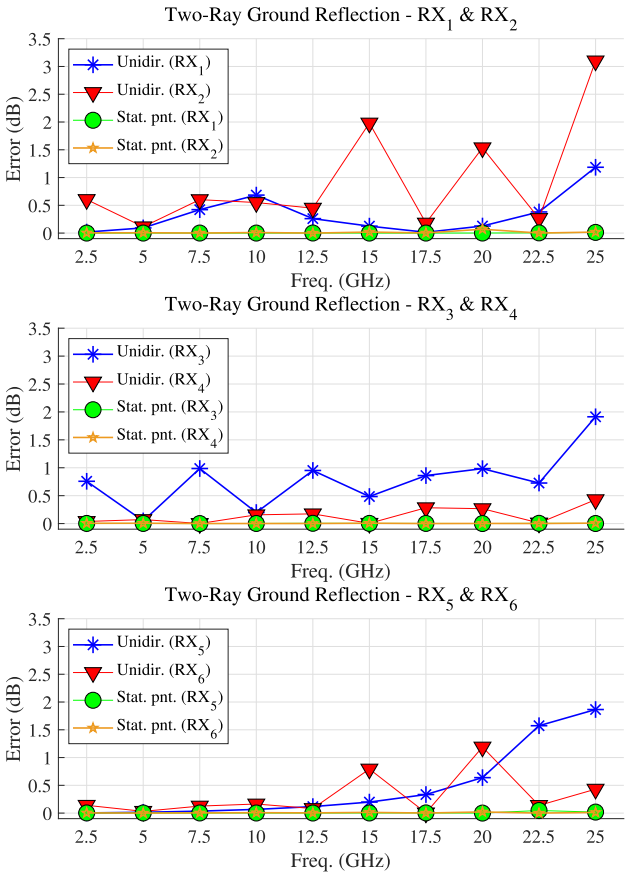

Fig. 8. Two-ray ground reflection scenario results.

The results indicate that utilizing a reception sphere of constant size yields a phase error in general when the operating frequency is changed from 2.5 to 25 GHz. However, the variation of the error is usually irregular, i.e., the error may diminish as well between the two consecutive steps. It can also be observed that the error figures for the diffraction scenario are greater than that for the two-ray reflection case, which might be explained with the larger number of multipaths in the diffraction scenario (four paths compared to two) and the presence of the diffraction cylinder as a secondary source of phase error in addition to the reception sphere. On the other hand, the proposed method demonstrates a much better performance for all the frequencies in both scenarios, as the error plots remain below 0.5 dB. The number of the rays, which were traced during the entire simulation, is larger for the unidirectional ray-tracing since Keller cones were utilized. Hence, it can be stated that the proposed algorithm achieves better accuracy even though the total number of rays involved in the simulation is much smaller than that in unidirectional ray-tracing.

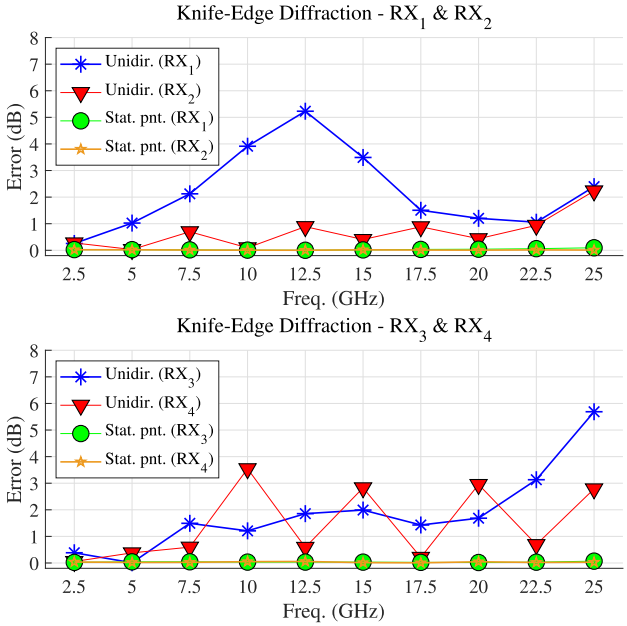

Fig. 9. Knife-edge diffraction scenario results.

B. Urban Scenario

A more practical propagation scenario based on a grid-like urban environment was simulated where realistic aspects and limitations of unidirectional ray-tracing simulations are emphasized to a greater extent. The scenario consists of five receivers and a transmitter, surrounded by concrete building blocks (see Fig. 7). Multipaths with up to seven reflections were considered (diffractions and refractions were omitted) and an operating frequency of 25 GHz was assumed. The discrepancy of the antenna transfer function with respect to a reference simulation was considered as the performance criterion, similar to Section V-B. Three distinct simulation cases were investigated.

Case I: The computational complexity of a typical simulation with the proposed algorithm is compared to that with conventional ray-tracing under similar accuracy constraints.

1) Simulation with the proposed method under the constraint that the deviation from the reference is below 0.5 dB for all receivers.
2) Unidirectional ray-tracing simulation with the same accuracy constraint as in *(a)*, i.e., no more than 0.5 dB error for any of the receiver.

The size of the reception sphere and the number of the ray launches in the unidirectional ray-tracing simulation were

Authorized licensed use limited to: University at Buffalo Libraries. Downloaded on October 08,2023 at 04:39:01 UTC from IEEE Xplore. Restrictions apply.

altered accordingly, i.e., sphere radius large enough to reduce the required number of ray launches, but small enough to prevent incorrect ray contributions (note that the incorrect ray paths can be distinguished according to the data from the reference simulation) as well as large phase errors. Considering that the accuracy for both simulation techniques is already sufficiently good (error with respect to the reference is less than 0.5 dB), the computational complexity, i.e., the total number of ray launches, is utilized as the comparison metric here.

Case II: The accuracy of the two simulation approaches is compared when the total number of the ray launches is equal. Four simulations were performed.

1) Simulation with the proposed method with the same parameters as in Case I.*(a)*.
2) Unidirectional ray-tracing simulation with the same number of ray launches as in the proposed method.
3) Rerun of simulation *(a)* for 2.5 GHz, instead of 25 GHz.
4) Rerun of simulation *(b)* for 2.5 GHz, instead of 25 GHz.

Similar to the Case I, the sphere size in the unidirectional ray-tracing simulation was adjusted to capture only the correct ray contributions. Thus, the deviations from the reference mainly emanate from phase errors as the size of the reception spheres is relatively large compared to the wavelength. In order to comprehend the severity of the phase errors in millimeter-wave environments, the simulations were repeated for 2.5 GHz as well, where the phase error is expected to be much smaller.

Case III: Reference data, which can be utilized to compare the simulation results, usually do not exist in a real simulation most of the time, as opposed to the idealized situations in Cases I and II. Therefore, a common practice is to perform multiple simulations while increasing the number of ray launches at each successive step until the final result (e.g., transfer function) converges according to a certain criterion. The advantages of the proposed algorithm against the traditional ray-tracing under such unfavorable circumstances are demonstrated by three different simulations.

1) Simulation with the proposed method using the same parameters as in Case I.*(a)* and Case II.*(a)*
2) Unidirectional ray-tracing simulation with large reception spheres having a diameter of 4 m (which is same as the side length of the cubic interaction surfaces utilized in the stationary point finding algorithm.)
3) Unidirectional ray-tracing simulation with smaller reception spheres (radius of 0.48 m) where incorrect ray contributions are avoided.

The convergence of the simulations was attained by progressively increasing the number of ray launches (i.e., starting with 1 million rays and increasing by 1 million at each subsequent step) until the difference of the transfer function values for two successive simulations is less than 0.5 dB. The simulations *(b)* and *(c)* demonstrate how the incorrect ray contributions can affect the simulation results. Such contributions can easily be captured with a large reception sphere, whereas the small reception sphere case does not involve this phenomenon. It can be anticipated that the simulation accuracy might deteriorate even further due to phase errors since the size of the reception spheres is considerably larger than the wavelength.

TABLE I

PARAMETERS UTILIZED FOR THE URBAN SCENARIO SIMULATIONS

Case	f (GHz)	Total ray launches ($\times 10^6$)	Intr. surf. or recept. sph. size (m)
I.*(a)*	25	1.05 / 1.05 / 1.05 / 2.05 / 2.05*	Cubic intr. surf. side len. 4 for all RX
I.*(b)*		3 / 4 / 3 / 5 / 14	Sph. radius 0.36 / 0.48 / 0.36 / 0.24 / 0.12
II.*(a)*	25	1.05 / 1.05 / 1.05 / 2.05 / 2.05*	Cubic intr. surf. side len. 4 for all RX
II.*(b)*			Sph. radius 0.48 for all RX
II.*(c)*	2.5		Cubic intr. surf. side len. 4 for all RX
II.*(d)*			Sph. radius 0.48 for all RX
III.*(a)*	25	1.05 / 1.05 / 1.05 / 2.05 / 2.05*	Cubic intr. surf. side len. 4 for all RX
III.*(b)*		4 / 3 / 4 / 1 / 4	Sph. radius 2 for all RX
III.*(c)*		1 / 1 / 1 / 3 / 3	Sph. radius 0.48 for all RX

The data in each cell denote the corresponding parameter for 5 receivers separated by slash marks.
The number of the correct multipaths is found as 6 / 6 / 4 / 6 / 6 for $RX_{1,\ldots,5}$.
$*$: In bidirectional ray-tracing, 50,000 rays are launched from the receiver site.

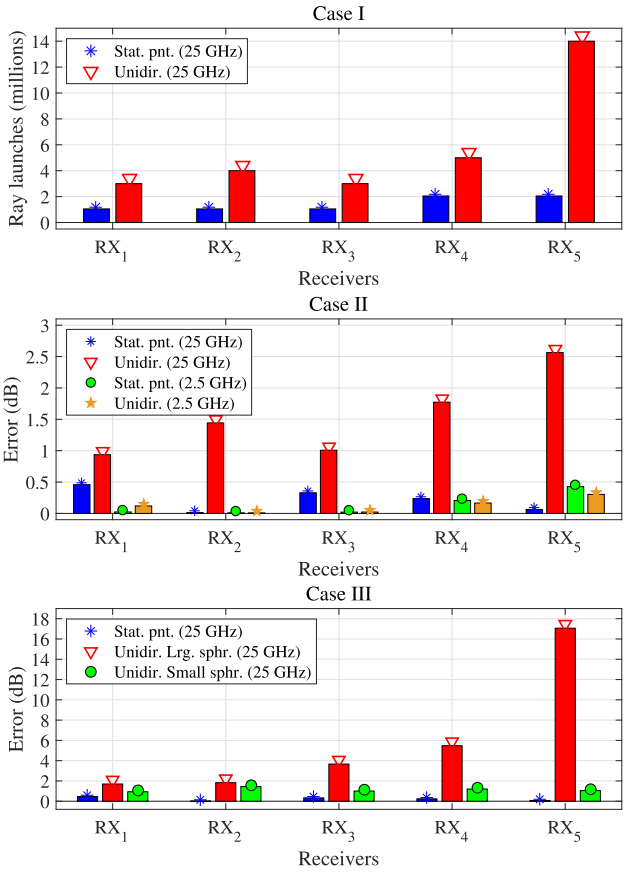

Fig. 10. Urban scenario results.

However, these effects will not be analyzed in this scenario, as they were considered in Case II.

The detailed simulation parameters for all simulations are presented in Table I, and the simulation results are shown in Fig. 10.

Authorized licensed use limited to: University at Buffalo Libraries. Downloaded on October 08,2023 at 04:39:01 UTC from IEEE Xplore. Restrictions apply.

The simulation results for Case I demonstrate that the total number of ray launches, which is needed to attain good accuracy (i.e., error less than 0.5 dB), is significantly different for the two simulation techniques. In the case of RX_5, the difference is as large as six times the number of rays which were utilized in the stationary point finding algorithm (14 million compared to 2.05 million). Even though the difference remains at relatively modest levels for the cases of other receivers, it is clearly visible that a larger number of ray launches is required in the unidirectional ray-tracing simulations in order to match the accuracy of the proposed approach.

The results for Case II reveal the detrimental effects of utilizing reception spheres of fixed size in unidirectional ray-tracing simulations for different frequencies, in a similar way that it was shown in the two-ray ground reflection and knife-edge diffraction scenarios. Two simulations, which were performed for 2.5 and 25 GHz, exhibit noticeable differences, although it was ensured that incorrect ray paths do not impair the outcome. Therefore, it can be concluded that phase errors are likely to be the reason for the deviations at 25 GHz, and that the simulation results in unidirectional ray-tracing can easily become erroneous with a small number of ray launches and large reception spheres, even if idealized circumstances, such as avoidance of the incorrect ray contributions, were established. On the other hand, our method shows small errors for both 2.5 and 25 GHz, indicating that the algorithm is very promising for a large range of frequencies.

The results of Case III exhibit the errors which might occur not only due to phase mismatch but also due to incorrect ray contributions. Here, more realistic circumstances are reproduced by letting the reception sphere to collect incorrect ray contributions. Evidently, the presence of incorrect ray paths degrades the accuracy dramatically, as the error can reach up to 17 dB. The presence of incorrect ray contributions has arguably delayed the convergence as well since the number of the rays utilized to achieve convergence is larger in the simulation *(b)* than in *(c)*. Note the stationary point algorithm [see *(a)*] outperforms the unidirectional ray-tracing method [see *(b)* and *(c)*] in terms of computational complexity as the total number of ray launches is usually smaller in *(a)*. More importantly, incorrect ray contributions do not affect the final accuracy in *(a)*, even though the size of the interaction surface is comparable to that of the reception sphere in *(b)*. Our algorithm thus provides here crucial flexibility compared to the conventional approach, as the size of the interaction surface can be varied in a much more flexible manner without accuracy issues.

C. Performance Comparison

Although the proposed method shares many common steps with the conventional bidirectional ray-tracing approach utilized in [4], a distinctive advantage of the new method is the computationally efficient integration based on an asymptotic expansion. To demonstrate the merits of this approach, the integration times of both methods are compared in Fig. 11 for the first receiver configuration in the urban scenario (RX_1) depicted in Fig. 7. In addition, the received power and the phases of the receiver voltages are also shown in Fig. 11.

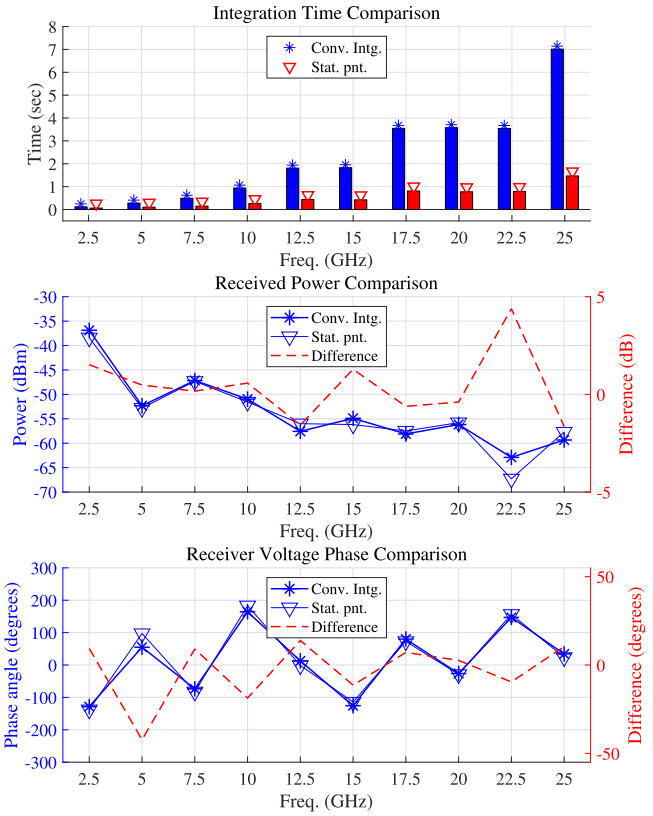

Fig. 11. Comparison of the proposed method with the traditional integration approach utilized in the bidirectional ray-tracing approach in [4].

The results indicate that the received voltage/power can be computed accurately with both integration schemes, as the discrepancies in the received power and the phase of the received voltage are relatively small. However, the computation time of the reciprocity integral for the two approaches shows a drastic difference. The integration time for the conventional technique is approximately four times larger than that for the stationary phase method. Since many wavefront pairs, which are time-consuming to process with the conventional method at higher frequencies, yield a stationary phase point, much smaller integration times can be achieved by employing the asymptotic approach.

VI. Conclusion

A novel algorithm to overcome problems with phase errors of millimeter-wave propagation and incorrectly detected rays in unidirectional ray-tracing approaches was presented. The method identifies the properties of the exact ray paths between two antennas on an interaction surface in accordance with the Fermat principle of least time, i.e., by minimizing the ray path length. The transfer function is then computed according to stationary phase approximation of the reciprocity integral where possible. The method was successfully demonstrated for three different problems. Furthermore, it was shown that some of the Keller cones in diffraction scenarios can be avoided by properly aligning the interaction surface. Thus, considerable

Authorized licensed use limited to: University at Buffalo Libraries. Downloaded on October 08,2023 at 04:39:01 UTC from IEEE Xplore. Restrictions apply.

improvements in the simulation complexity can be achieved without compromising the accuracy.

REFERENCES

[1] F. Hossain *et al.*, "An efficient 3-D ray tracing method: Prediction of indoor radio propagation at 28 GHz in 5G network," *Electronics*, vol. 8, no. 3, p. 286, 2019.

[2] N. Hirsenkorn *et al.*, "A ray launching approach for modeling an FMCW radar system," in *Proc. 18th Int. Radar Symp. (IRS)*, Prague, Czech Republic, Jun. 2017, pp. 1–10.

[3] H. Ling, R.-C. Chou, and S.-W. Lee, "Shooting and bouncing rays: Calculating the RCS of an arbitrarily shaped cavity," *IEEE Trans. Antennas Propag.*, vol. 37, no. 2, pp. 194–205, Feb. 1989.

[4] M. M. Taygur, I. O. Sukharevsky, and T. F. Eibert, "A bidirectional ray-tracing method for antenna coupling evaluation based on the reciprocity theorem," *IEEE Trans. Antennas Propag.*, vol. 66, no. 12, pp. 6654–6664, Dec. 2018.

[5] T. Chao-han, S. Dan, S. Yuqi, and G. You-gang, "The application of an improved SBR algorithm in outdoor environment," in *Proc. 7th Asia–Pacific Conf. Environ. Electromagn. (CEEM)*, Hangzhou, China, Nov. 2015, pp. 359–363.

[6] V. Mohtashami and A. A. Shishegar, "Efficient shooting and bouncing ray tracing using decomposition of wavefronts," *IET Microw., Antennas Propag.*, vol. 4, no. 10, pp. 1567–1574, Oct. 2010.

[7] M. Schiller, A. Knoll, M. Mocker, and T. Eibert, "GPU accelerated ray launching for high-fidelity virtual test drives of VANET applications," in *Proc. Int. Conf. High Perform. Comput. Simulation (HPCS)*, Amsterdam, The Netherlands, Jul. 2015, pp. 262–268.

[8] D. Shi, J. J. Bi, Z. L. Tan, and Y. G. Gao, "Site-specific wave propagation prediction with improved shooting and bouncing ray tracing method," in *Proc. 1st URSI Atlantic Radio Sci. Conf. (URSI AT-RASC)*, Las Palmas, Spain, May 2015, p. 1.

[9] V. Mohtashami and A. A. Shishegar, "Accuracy and computational efficiency improvement of ray tracing using line search theory," *IET Microw., Antennas Propag.*, vol. 4, no. 9, p. 1290, Sep. 2010.

[10] J. Shen and Y. Li, "Light ray optimization and its parameter analysis," in *Proc. Int. Joint Conf. Comput. Sci. Optim.*, Sanya, China, Apr. 2009, pp. 918–922.

[11] S. Vogt, J. Jebramcik, O. Garten, J. Barowski, and I. Rolfes, "Investigation on optical methods for multi scale electromagnetic simulations," in *Proc. 12th German Microw. Conf. (GeMiC)*, Stuttgart, Germany, Mar. 2019, pp. 28–31.

[12] M. M. Taygur, I. O. Sukharevsky, and T. F. Eibert, "Computation of antenna transfer functions with a bidirectional ray-tracing algorithm utilizing antenna reciprocity," in *Proc. 2nd URSI Atlantic Radio Sci. Meeting (AT-RASC)*, Gran Canaria, Spain, May 2018, pp. 1–4.

[13] R. Brem and T. F. Eibert, "A shooting and bouncing ray (SBR) modeling framework involving dielectrics and perfect conductor," *IEEE Trans. Antennas Propag.*, vol. 63, no. 8, pp. 3599–3609, Aug. 2015.

[14] Z. Yun and M. F. Iskander, "Ray tracing for radio propagation modeling: Principles and applications," *IEEE Access*, vol. 3, pp. 1089–1100, 2015.

[15] S. Y. Seidel and T. S. Rappaport, "A ray tracing technique to predict path loss and delay spread inside buildings," in *Proc. Global Telecommun. Conf.*, Orlando, FL, USA, Dec. 1992, pp. 649–653.

[16] D. Didascalou, T. M. Schafer, F. Weinmann, and W. Wiesbeck, "Ray-density normalization for ray-optical wave propagation modeling in arbitrarily shaped tunnels," *IEEE Trans. Antennas Propag.*, vol. 48, no. 9, pp. 1316–1325, Sep. 2000.

[17] D. Popmintchev and T. Popmintchev, *Introduction to Design of Optical Systems*, 2018. [Online]. Available: https://play.google.com/store/books/details?id=xd9VDwAAQBAJ

[18] M. Born and E. Wolf, *Principles of Optics: Electromagnetic Theory of Propagation, Interference and Diffraction of Light*. Cambridge, U.K.: Cambridge Univ. Press, 2013.

[19] M. M. Taygur, I. O. Sukharevsky, and T. F. Eibert, "Investigation of massive MIMO scenarios involving rooftop propagation By bidirectional ray-tracing," *Prog. Electromagn. Res. C*, vol. 91, pp. 129–142, 2019.

[20] C. A. Balanis, "Antenna theory: A review," *Proc. IEEE*, vol. 80, no. 1, pp. 7–23, Jan. 1992.

[21] R. Collin and F. Zucker, *Antenna Theory*. New York, NY, USA: McGraw-Hill, 1969.

[22] R. V. Gamkrelidze, *Analysis I: Integral Representations Asymptotic Methods*. Berlin, Germany: Springer, 2011.

[23] S. Olver, "Numerical approximation of highly oscillatory integrals," Ph.D. dissertation, Dept. Math., Univ. of Cambridge, Cambridge, U.K., 2008.

[24] A. Asheim, "Numerical methods for highly oscillatory problems," Ph.D. dissertation, Dept. Math. Sci., NTNU, Trondheim, Norway, 2010.

[25] M. V. Fedoryuk, "The stationary phase method and pseudodifferential operators," *Russian Math. Surv.*, vol. 26, no. 1, pp. 65–115, Feb. 1971.

[26] R. Wong, *Asymptotic Approximations Integrals*. Philadelphia, PA, USA: SIAM, 2001.

[27] M. R. Kumar and G. Uthra, "A study on numerical stability of finite difference formulae for numerical differentiation and integration," *Ann. Pure Appl. Math.*, vol. 8, no. 2, pp. 27–36, Dec. 2014.

[28] S. D. Conte and C. de Boor, *Elementary Numerical Analysis: An Algorithmic Approach*. New York, NY, USA: McGraw-Hill, 1980.

[29] J. Keller, "Geometrical theory of diffraction," *J. Opt. Soc. Amer.*, vol. 52, no. 2, pp. 116–130, Feb. 1962.

Mehmet Mert Taygur (Member, IEEE) received the B.Sc. and M.Sc. degrees in electrical and electronics engineering from Dokuz Eylül University, Izmir, Turkey, in 2012 and 2014, respectively.

He is currently a Research Assistant with the Chair of High-Frequency Engineering, Technical University of Munich, Munich, Germany. His current research interests include asymptotic techniques in electromagnetics, computing on graphical processing units, and massive multiple-input multiple-output systems.

Thomas F. Eibert (Senior Member, IEEE) received the Dipl.-Ing. (FH) degree in electrical engineering from Fachhochschule Nürnberg, Nuremberg, Germany, in 1989, the Dipl.-Ing. degree in electrical engineering from Ruhr-Universität Bochum, Bochum, Germany, in 1992, and the Dr.-Ing. degree in electrical engineering from Bergische Universität Wuppertal, Wuppertal, Germany, in 1997.

He is currently a Full Professor of high-frequency engineering with the Technical University of Munich, Munich, Germany.

Authorized licensed use limited to: University at Buffalo Libraries. Downloaded on October 08,2023 at 04:39:01 UTC from IEEE Xplore. Restrictions apply.